MITSUBISHI ELECTRIC RESEARCH LABORATORIES
https://www.merl.com

Control Co-Design for Electric Vehicles with Driving Cycle Synthesis Encoding Road Traffic and Driver Characteristics

Park, Seho; Wang, Yebin; Qiao, Hongtao; Sakamoto, Yusuke; Wang, Bingnan; Liu, Dehong

TR2024-114 August 29, 2024

Abstract

This paper employs the control co-design paradigm to determine optimal motor size and optimal Heating Ventilation Air Conditioning (HVAC) control for system-level optimal performance of electric vehicle. Our work is motivated by the realization that whether an electric vehicle design and its control strategy best fit consumer depends on who operates it, where and how it is operated. To this end, we first propose a novel method to synthesize a customer-specific driving cycle which encodes traffic information and driver characteristics, effectively addressing where and by whom the electric vehicle is operated; then conduct physics-based model reduction and data-driven modeling for motor sizing and HVAC control design; and apply established control co-design approaches to jointly optimize the motor size and HVAC power control for a given driving cycle, addressing how it is operated. The proposed method is validated by performing electric motor design and open-loop HVAC control in numerical simulation, showcasing that the control co-design practice leads to an appropriate combination of motor size and HVAC control and more efficient operation for the given customer-specific driving cycle.

IEEE Conference on Control Technology and Applications (CCTA) 2024

Mitsubishi Electric Research Laboratories, Inc.
201 Broadway, Cambridge, Massachusetts 02139

Control Co-Design for Electric Vehicles with Driving Cycle Synthesis Encoding Road Traffic and Driver Characteristics

Seho Park, Yebin Wang, Hongtao Qiao, Yusuke Sakamoto, Bingnan Wang, and Dehong Liu

***Abstract*— This paper employs the control co-design paradigm to determine optimal motor size and optimal Heating Ventilation Air Conditioning (HVAC) control for system-level optimal performance of electric vehicle. Our work is motivated by the realization that whether an electric vehicle design and its control strategy best fit consumer depends on who operates it, where and how it is operated. To this end, we first propose a novel method to synthesize a customer-specific driving cycle which encodes traffic information and driver characteristics, effectively addressing where and by whom the electric vehicle is operated; then conduct physics-based model reduction and data-driven modeling for motor sizing and HVAC control design; and apply established control co-design approaches to jointly optimize the motor size and HVAC power control for a given driving cycle, addressing how it is operated. The proposed method is validated by performing electric motor design and open-loop HVAC control in numerical simulation, showcasing that the control co-design practice leads to an appropriate combination of motor size and HVAC control and more efficient operation for the given customer-specific driving cycle.**

I. Introduction

Plant and controller designs for a system are often carried out separately: design parameters for the plant are optimized first and then followed by designing an optimal controller for the given plant to achieve optimal performance [1], [2]. This sequential procedure may not capture the system-level optimality since the optimal plant parameters and optimal control parameters are generally coupled with each other [3]. Specifically, the optimal control parameter is subject to the system dynamics and constraints, affected by the plant parameters while the optimal plant parameter is dependent on the control parameters. Hence, optimal design for the plant and controller should be considered simultaneously for system-level performance optimization [4]–[6].

Another consideration for optimal plant and controller design is disturbance (including reference) that the system has to deal with. System feasibility and performance are influenced by the disturbance, and thus the plant and controller should be designed to operate the system successfully and obtain optimal performance under disturbances. For the optimization of electrified vehicle efficiency, one critical disturbance is the driving cycle [7]. Generally, representative driving cycles such as UDDS and US06 have been adopted to evaluate the plant and controller design [8], [9] but sometimes they do not reflect real-world driving cycles involving road traffic demand as well as driver's characteristics [10].

For real-world driving cycles, naturalistic driving cycle synthesis has been developed with statistical features [11], [12]. However, these methods require experiment data and data processing to deal with missed and noisy data [13]. Additionally, general driving cycles describe velocity profiles from the macroscopic perspective such as traffic flow. These may not be matched with the practical situations as it does not involve driver characteristics, which can compromise the feasibility and performance of the systems designed with plant and controller on the driving cycles neglecting driver characteristics. Driver modeling with microscopic traffic flow models [14] have been studied to describe driver characteristics but their application to vehicle design and control has not been extensively discussed.

Previous studies have employed a control co-design framework with approximately scaled models to obtain optimal design and control [15]–[18]. With the overly-simplified models, plant design parameter space can be easily constructed albeit along with compromised system feasibility and performance by underestimating physics (e.g., efficiency map). Work [17] aims to improve energy economy of electric vehicle by exploiting the design freedom in sizes of dual motors and control freedom in the torque-split ratio between motors as well as the velocity profile. Work [18] determines motor sizes, transmission ratios as well as torque-allocation strategy among two motors. However the motor size is characterized by its rated power and the efficiency map is assumed constant in [17], [18].

This paper applies a control co-design framework to find the optimal design of an electric motor and the optimal Heating Ventilation Air Conditioning (HVAC) control for energy economy of electric vehicles. Our contributions are: 1) deriving a reduced-order model (implying motor efficiency map) and constraints of an electric motor, which is differentiable w.r.t. the design parameters and thus allows efficient design optimization; 2) following a physics- and data-driven modeling to establish the HVAC power consumption model; 3) proposing a novel method to synthesize a driver-specific real-world driving cycle to reflect driver characteristics as well as road traffic situations in a simulation environment

S. Park is with the Dept. of Mechanical Engineering, The Pennsylvania State University, University Park, PA 16802, USA. This work was done while S. Park was a research intern at Mitsubishi Electric Research Laboratories (MERL), Cambridge, MA 02139, USA. (Email: sehopark@psu.edu).

Y. Wang, H. Qiao, B. Wang, and D. Liu are with MERL. (Email: {yebinwang,qiao,bwang,liudh}@merl.com).

Y. Sakamoto is with Advanced Technology R&D Center, Mitsubishi Electric Corporation, Amagasaki City, Japan. (Email: sakamoto.yusuke@df.mitsubishielectric.co.jp)

using SUMO [19] and OpenStreetMap [20], thus mitigating experiment data requirements and making procedures efficient; 4) employing established approaches to co-design motor size and HVAC control of electric vehicle; 5) performing numerical simulation to validate the proposed method.

The remainder of this paper is organized as follows. Section II introduces the control co-design problem. Section III describes the driving cycle synthesis procedure with driver characteristics and presents electric vehicle model and control co-design schemes. Section IV shows the proposed method results via numerical simulation. Section V provides concluding remarks.

II. Control Co-Design Problem and Nested Approach

The joint optimization of control and design parameters for system-level optimization is called control co-design. It typically admits a cost function in the form of

$$J(x_p, u) = J_p(x_p) + J_c(x_p, u)\,, \tag{1}$$

where x_p and u are system design parameters and control inputs, respectively, and $J_p, J_c = \int_0^{t_f} \mathcal{L}(x_p, u(t))\mathrm{d}t$ are costs for design optimization and control optimization, respectively. Given (1), the control co-design problem can be formulated as

$$\begin{aligned}
\underset{x_p,u}{\text{minimize}} \quad & J(x_p, u)\,, && \text{(2a)}\\
\text{subject to} \quad & \dot{z}(t) = f(z(t), u(t), d(t); x_p)\,, && \text{(2b)}\\
& c(x_p, z(t), u(t)) \le 0\,, && \text{(2c)}\\
& h(x_p) = 0\,, && \text{(2d)}\\
& g(x_p) \le 0\,, && \text{(2e)}
\end{aligned}$$

where z and d are system states and disturbances, respectively, and $u(t)$ is the control inputs at time t. By applying the Pontryagin's Maximum Principle, one can derive the necessary optimality conditions for (1) and appreciate the interdependence between design optimization and control optimization [3], which entails the control co-design.

To obtain the optimal solution of (2), it should be solved over both x_p and u simultaneously. However, this formulation demands huge computational complexity. Alternatively, iterative [21], [22] and nested frameworks [6] are often used to solve the problem by decomposing the control co-design problem into two subproblems: design optimization and control optimization. Since the nested framework can handle the coupling between design and control optimization more, it is adopted in this study.

The nested approach consists of an outer loop and an inner loop. The outer loop, given control u^*, optimizes design x_p:

$$\begin{aligned}
\underset{x_p}{\text{minimize}} \quad & J(x_p, u^*)\,, && \text{(3a)}\\
\text{subject to} \quad & u^*(t) \text{ is given by the inner loop (4)}\,, && \text{(3b)}\\
& h(x_p) = 0\,, && \text{(3c)}\\
& g(x_p) \le 0\,. && \text{(3d)}
\end{aligned}$$

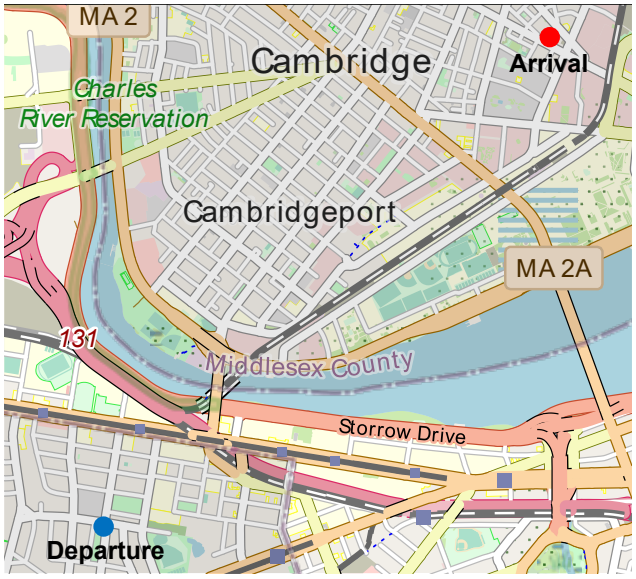

Fig. 1: The area of interest in Boston for driving cycle synthesis.

and the inner loop optimizes control u with given design x_p^*:

$$\begin{aligned}
\underset{u}{\text{minimize}} \quad & J(x_p^*, u)\,, && \text{(4a)}\\
\text{subject to} \quad & x_p^* \text{ is given by the outer loop (3)}\,, && \text{(4b)}\\
& \dot{z}(t) = f(z(t), u(t), d(t); x_p^*)\,, && \text{(4c)}\\
& c(x_p^*, z(t), u(t)) \le 0\,. && \text{(4d)}
\end{aligned}$$

The nested framework is iteratively implemented until the optimization problem converges to the optimal value.

III. Control Co-Design for Electric Vehicles

This section presents a method to synthesize a driving cycle which effectively encodes traffic information and driver characteristics, the vehicle model dynamics accounted for motor sizing and HVAC control co-design, and the sequential and nested approaches to solve the proposed control co-design of motor size and HVAC control.

A. Driving Cycle Synthesis

Driving cycles are location-specific, i.e., depending on road types (e.g., urban and highway) and traffic situations (e.g., traffic lights and the number of vehicles). Generally, representative driving cycles for urban and highway roads (e.g., UDDS and US06) have been widely employed for vehicle design and control validation purposes since they can imply some properties of typical roads. Nevertheless, the representative driving cycles do not adequately capture real-world driving cycles of a particular driver such as daily driving schedules and short/long commute driving schedules.

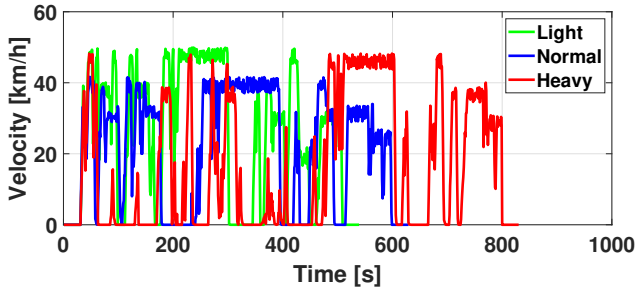

Fig. 2: Driving cycles of the same route in the area of interest with different traffic demands.

For real-world driving cycle synthesis, we use a traffic simulator (SUMO) [19] with OpenStreetMap [20], which can reflect the traffic situations in an area of interest. It can generate a specific area map with traffic situations (e.g., traffic lights, vehicle types, and traffic demands). For a case study, the Boston area shown in Fig. 1 is considered as the area of interest and the driving cycles shown in Fig. 2 are generated to represent a commute scenario from the Departure to the Arrival on the map. It includes traffic lights and several traffic demands of passenger vehicles, buses, trains, bicycles, and pedestrians. The driving cycles in Fig. 2 show driving cycles for the same route in Fig. 1 w.r.t. light, normal, and heavy traffic demands. As the traffic demand increases, the trip duration and stopping period get longer.

There are two options for driving cycle synthesis with SUMO and OpenStreetMap. First, users can generate traffic demands using SUMO with the extracted information on the area of interest such as how many lanes on the road, the number of traffic lights, and the duration of traffic light signals by OpenStreetMap. However, this approach is computationally demanding and appropriate for small networks and specific traffic demands.

Second, SUMO supports an algorithm that can generate random traffic demands on the map. The traffic demands (how many vehicles are generated per hour on the map and their routes are randomly defined) can be adjusted by "Counter" parameter in the SUMO application. This is more appropriate for large networks and users can generate their interesting traffic demands in the area of interest. By using the traffic control interface supported [23] by SUMO, several signals (e.g., vehicle velocity, acceleration, and the number of vehicles on the network) can be obtained with MATLAB or Python. The second approach is adopted in this study due to its simplicity and scalability.

B. Driver Model

In addition to driving cycles, drivers have different driving styles, for example, cautious and aggressive driving styles based on the driver characteristics, which is expected to impact the motor size and HVAC control strategy. The driver characteristics can be described with a car-following scenario, representing how quickly the driver tries to accelerate and decelerate following the preceding vehicle. We modeled

TABLE I: Vehicle parameters

Description	Value
Vehicle Mass	1080 kg
Aerodynamic Drag Coefficient	0.35
Frontal Area	2.37 m^2
Rolling Resistance Coefficient	0.015
Final Gear Ratio	6.06
Motor Speed Range	0 – 8000 rpm
Motor Torque Range	-180 N·m – 180 N·m

the driver characteristics with the optimal velocity model (OVM) [14], which can be described as

$$\begin{aligned} \frac{\mathrm{d}x}{\mathrm{d}t} &= v, \\ \frac{\mathrm{d}v}{\mathrm{d}t} &= \alpha \left(V_{\text{opt}}(\Delta x(t)) - v(t) \right), \\ V_{\text{opt}}(\Delta x(t)) &= v_{\max}(\tanh(\beta(x_{\text{pre}}(t) - x(t)) - \gamma) + 1), \end{aligned} \tag{5}$$

where V_{opt} is a function mapping the relative distance to velocity, α is the driver sensitivity. β and γ are the slope and the intercept of $\tanh$ function. $\Delta x(t)$, $x_{\text{pre}}(t)$, $x(t)$, and $v(t)$ are relative distance to the preceding vehicle, preceding vehicle location, ego vehicle location, and vehicle velocity, respectively. One can generate $x_{\text{pre}}(t)$ from the driving cycles shown in Fig. 2 and feed it into (5) with certain values of α, β and γ to generate the driver-specific driving cycle $v(t)$. The driving cycle $v(t)$, encoding traffic information and driver characteristics, will be used to direct the following co-design of motor size and HVAC control strategy.

C. Electric Vehicle Model and HVAC Control

A Mitsubishi innovative electric vehicle (MiEV) is considered as a benchmark model for this study. The vehicle parameters are described in Table I. An interior permanent synchronous motor is used for the propulsion of electric vehicle. It is well-known that detailed motor design, involving finite element analysis of electromagnetics, mechanics and thermal dynamics, is highly complicated and time-consuming. For simplicity, we assume the presence of a reference motor with a fixed 2D geometry of its cross-section and shaft length as shown in Fig. 14 in Appendix.

We propose to represent a new motor design by parameter vector $x_p := [k_r, k_k]^\top$, which scales the radius and shaft of a pre-selected reference motor by k_r and k_l, respectively. The reference motor has the electrical model parameters $(\Phi_{m0}, L_{d0}, L_{q0}, R_0, k_{\text{hyst0}}, k_{\text{eddy0}}, M_{\text{motor0}})$, denoting the permanent magnet flux, d-axis inductance, q-axis inductance, stator winding resistance, hysteresis loss coefficient, eddy current loss coefficient, and motor mass, respectively. Given a scaled motor design x_p, the electrical model parameters of the scaled motor can be updated based on those of the reference motor as follows

$$\begin{aligned} \Phi_m = k_r k_l \Phi_{m0}\ , L_d = k_l L_{d0}\ L_q = k_l L_{q0}\ , \\ k_{\text{hyst}} = k_r^2 k_l k_{\text{hyst0}}\ , k_{\text{eddy}} = k_r^2 k_l k_{\text{eddy0}}, \\ M_{\text{motor}} = k_r^2 k_l M_{\text{motor0}},\ \ R = \frac{R_0}{k_r}. \end{aligned} \tag{6}$$

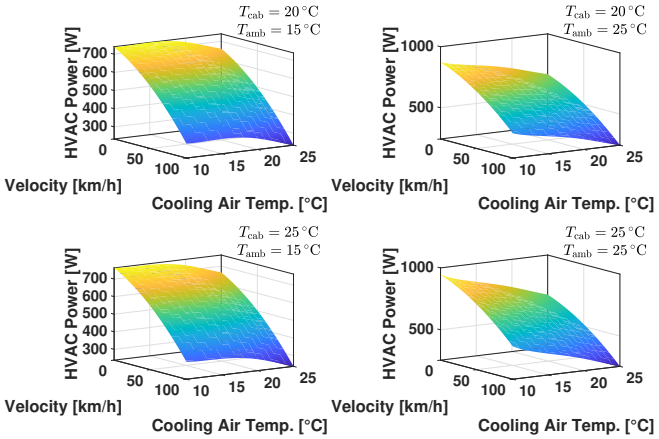

Fig. 3: Control-oriented HVAC power consumption map.

The detailed derivation of formulas (6) can be found in Appendix. The physics-based modeling in Appendix allows us to establish analytically mappings from design parameters to key metrics of motor such as weight, torque capacity, losses, and efficiency.

The HVAC control objective is to regulate the cabin temperature within the defined range and minimize the battery energy consumption consisting of propulsive motor power, HVAC power and battery losses. The cabin temperature dynamics are formulated as

$$\begin{aligned} M_{\text{cab}} c_{\text{clnt}} \frac{\mathrm{d}T_{\text{cab}}}{\mathrm{d}t} &= -\dot{m}_{\text{clnt}} c_{\text{clnt}} (T_{\text{cab}} - T_{\text{clnt}}) \\ &\quad - K(T_{\text{cab}} - T_{\text{amb}}) + Q_{\text{rad}} + Q_{\text{psgr}} + Q_{\text{loss}}, \end{aligned} \tag{7}$$

where T_{cab}, T_{amb}, and T_{clnt} are cabin, coolant, and ambient temperatures, respectively. M_{cab}, c_{clnt}, $\dot{m}_{\text{clnt}}$, Q_{rad}, Q_{psgr}, and Q_{loss} are cabin air mass, air specific heat, air flow rate, solar radiation, passenger heat generation, and motor power loss respectively. K is the ambient heat transfer coefficient, which is a function of vehicle speed. In order to derive the HVAC power consumption model, we first assume the HVAC system operates at steady-state and derive a reduced-order HVAC system model in the form of nonlinear algebraic equations, and then generate the optimal power consumption dataset for different operation conditions characterized by $(T_{\text{cab}}, T_{\text{clnt}}, T_{\text{amb}}, v)$. Since the reduced-order model has multiple control variables: compressor speed, cabin fan speed and radiator fan speed, we determine the optimal HVAC power consumption by optimization for a given operation point. Finally, given the dataset of P_{HVAC} and the respective operation conditions $(T_{\text{cab}}, T_{\text{clnt}}, T_{\text{amb}}, v)$, via polynomial approximation, we obtain the map from $(T_{\text{cab}}, T_{\text{clnt}}, T_{\text{amb}}, v)$ to HVAC power as $P_{\text{HVAC}} = f_{\text{HVAC}}(T_{\text{cab}}, T_{\text{clnt}}, T_{\text{amb}}, v)$. Fig. 3 shows snapshots of $f_{\text{HVAC}}(T_{\text{cab}}, T_{\text{clnt}}, T_{\text{amb}}, v)$ for illustration purpose.

D. Sequential Approach

The optimal motor design and controller synthesis for a given driving cycle of time $t \in [0, t_f]$ are performed sequentially. The former is obtained by minimizing motor loss while satisfying motor physical constraints as follows

$$\begin{aligned} \underset{x_p, u_m}{\text{minimize}} \quad & \int_0^{t_f} P_{\text{motor,loss}}(v, u_m; x_p)\mathrm{d}t, && \text{(8a)} \\ \text{subject to} \quad & \dot{v} = f_{\text{veh}}(v, \tau_{\text{motor}}; x_p), && \text{(8b)} \\ & \tau_{\text{motor}} = \frac{3p}{2}(\Phi_m + (L_d - L_q) i_d) i_q, && \text{(8c)} \\ & (L_q i_q)^2 + (\Phi_m + L_d i_d)^2 \le \left(\frac{V_{\max}}{p\omega}\right)^2, && \text{(8d)} \\ & i_d^2 + i_q^2 \le i_{\max}^2, && \text{(8e)} \\ & 0.2 \le x_p \le 5, && \text{(8f)} \end{aligned}$$

where $u_m(t) := [i_d(t), i_q(t)]^\top$ denotes motor control to meet the propulsive demand, v and $f_{\text{veh}}(v, \tau_{\text{motor}}; x_p)$ are the vehicle speed and longitudinal dynamics, respectively, i_d, i_q, p, $i_{\max}$, and $V_{\max}$ are d-axis current, q-axis current, the number of pole pairs, and maximum current, maximum voltage, respectively; and ω is the motor speed. $P_{\text{motor,loss}}$ is motor loss and can be modeled as $P_{\text{motor,loss}} = P_{\text{copper,loss}} + P_{\text{hyst,loss}} + P_{\text{eddy,loss}}$. Specifically, $P_{\text{copper,loss}}$, $P_{\text{hyst,loss}}$, and $P_{\text{eddy,loss}}$ denote copper loss, hysteresis loss, and eddy loss, respectively and are given by

$$\begin{aligned} P_{\text{copper,loss}} &= \frac{3}{2} R(i_d^2 + i_q^2), \\ P_{\text{hyst,loss}} &= k_{\text{hyst}} \Phi \frac{p\omega}{2\pi}, \; P_{\text{eddy,loss}} = k_{\text{eddy}} \Phi \left(\frac{p\omega}{2\pi}\right)^2, \\ \Phi &= \sqrt{(L_q i_q)^2 + (\Phi_m + L_d i_d)^2}. \end{aligned} \tag{9}$$

The motor speed ω is linearly proportional to the vehicle speed v with the ratio regulated by the gearbox.

With the obtained motor design by solving (8), controller synthesis problem is formulated as follows

$$\begin{aligned} \underset{u}{\text{minimize}} \quad & \int_0^{t_f} P_{\text{batt}}(z, u; x_p^*)\mathrm{d}t, && \text{(10a)} \\ \text{subject to} \quad & \dot{z} = f_{\text{dyn}}(z, u; x_p^*), && \text{(10b)} \\ & x_p^* \text{ is given by the design optimization (8)}, && \text{(10c)} \\ & T_{\text{cab,min}} \le T_{\text{cab}} \le T_{\text{cab,max}}, && \text{(10d)} \\ & T_{\text{clnt,min}} \le T_{\text{clnt}} \le T_{\text{clnt,max}}, && \text{(10e)} \end{aligned}$$

where $z := [v, T_{\text{cab}}]^\top$ is system state, $f_{\text{dyn}} := [(8b),\ (7)]^\top$ system dynamics, and $u := T_{\text{clnt}}$ is control input. P_{batt} is battery power composed of motor power ($P_{\text{motor}} = \tau_{\text{motor}}\omega + P_{\text{motor,loss}}$), HVAC power $f_{\text{HVAC}}(T_{\text{cab}}, T_{\text{clnt}}, T_{\text{amb}}, v)$, and battery loss given by $I_{\text{batt}}^2 R_{\text{batt}}$ where $I_{\text{batt}} = (P_{\text{motor}} + P_{\text{HVAC}})/V_{\text{batt}}$ is the battery terminal current and R_{batt} is the battery internal resistance. Here V_{batt} is the battery terminal voltage. $T_{\text{cab,min}}$, $T_{\text{cab,max}}$, $T_{\text{clnt,min}}$, and $T_{\text{clnt,max}}$ denote minimum and maximum temperatures of cabin and coolant, respectively.

Remark 1: Given u_m as a solution of (8), motor power P_{motor} is fixed and can be eliminated. The cost function of controller synthesis problem can be simplified to $f_{\text{HVAC}}(T_{\text{cab}}, T_{\text{clnt}}, T_{\text{amb}}, v) + I_{\text{batt}}^2 R_{\text{batt}}$.

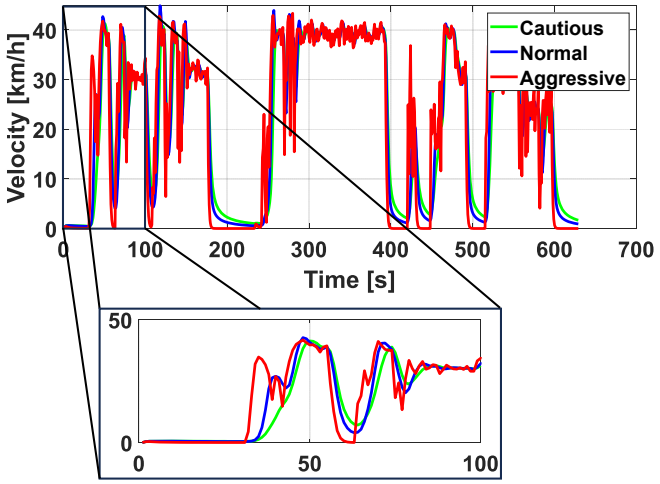

Fig. 4: Velocity trajectories of Driving Cycle A based on cautious, normal, and aggressive driver characteristics.

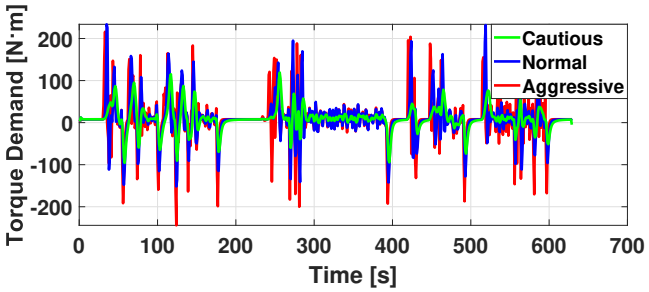

Fig. 5: Torque demand trajectories of Driving Cycle A for cautious, normal, and aggressive driver characteristics.

For optimal control performance, dynamic programming (DP) is applied to controller design. DP is generally used as a benchmark for ideally obtainable performance.

E. Nested Approach

1) Outer Loop of Nested Framework–Design Optimization: Motor sizing for a given driving cycle is stated as

$$\begin{aligned} \underset{x_p,u_m}{\text{minimize}} \quad & \int_0^{t_f} P_{\text{batt}}(z,u_m,u^*;x_p)\mathrm{d}t, \\ \text{subject to} \quad & \dot{z} = f_{\text{dyn}}(z,u_m,u^*;x_p), \\ & u^*(t) \text{ is given by the inner loop (12)}, \\ & \text{(8b)–(8f), (10d)–(10e)}, \end{aligned} \tag{11}$$

where u^* is the optimal HVAC control trajectory given by the inner loop (12). Here, the design optimization problem is formulated to minimize the battery energy consumption P_{batt} with respect to design parameter x_p and motor control u_m. The rationale to include u_m in the motor sizing problem is 1) to enforce the satisfaction of longitudinal dynamics for any new motor; 2) to ensure that all models and constraints in the resultant motor sizing problem are analytical and thus can be readily implemented in CasADi [24].

Remark 2: If following the traditional nested approach, the temperature constraints in (11) should not be imposed.

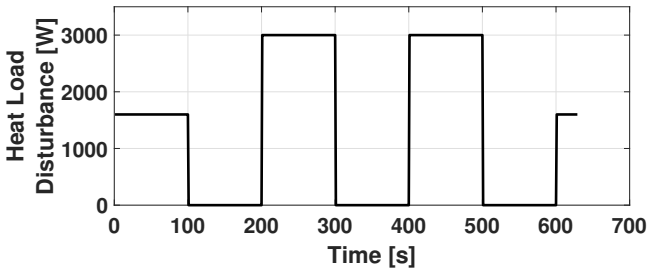

Fig. 6: Heat load disturbance trajectory to the vehicle cabin.

TABLE II: Optimized motor design of different drivers with control co-design approaches

Driver		Cautious	Normal	Aggressive
Base	k_r	1		
	k_l	1		
	Mass	50 kg		
Sequential	k_r	0.6	0.7	0.7
	k_l	4.5	4.6	4.7
	Mass	81 kg	112.7 kg	115.15 kg
Nested	k_r	0.4	0.5	0.5
	k_l	5	5	5
	Mass	40 kg	62.5 kg	62.5 kg

Here, we introduce them to ensure that the given HVAC control u^* remains feasible for new motor design.

2) Inner Loop of Nested Framework–Control Optimization: The control optimization is formulated as follows

$$\begin{aligned} \underset{u}{\text{minimize}} \quad & \int_0^{t_f} P_{\text{batt}}(z,u_m^*,u;x_p^*)\mathrm{d}t\,, \\ \text{subject to} \quad & \dot{z} = f_{\text{dyn}}(z,u_m^*,u;x_p^*)\,, \\ & x_p^* \text{ is given by the outer loop (11)}\,, \\ & \text{(10d)} - \text{(10e)}, \end{aligned} \tag{12}$$

Here, the optimal control trajectory is obtained and then given to the outer loop of nested framework. The outer loop and inner loop are iterated until convergence.

IV. Simulation

To validate the proposed approach, we examine the motor design and HVAC control on Driving Cycle A (the real-world driving cycle with normal traffic demand in Fig. 2) with three drivers (cautious, normal, and aggressive). Using (5), three different driving cycles for three drivers on Driving Cycle A are generated as shown in Fig. 4. The aggressive driver frequently and aggressively accelerates and decelerates in order to follow the preceding vehicle while the cautious driver drives more smoothly than the aggressive driver. The normal driver accelerates and decelerates between the aggressive driver and the cautious driver.

Fig. 5 shows torque demand trajectories for different driver characteristics and heat load disturbance to the cabin is shown in Fig. 6. The aggressive driver uses higher torque demand than normal and cautious drivers, which might not be realized with motors designed for normal and cautious drivers. Additionally, different torque demands entail more or

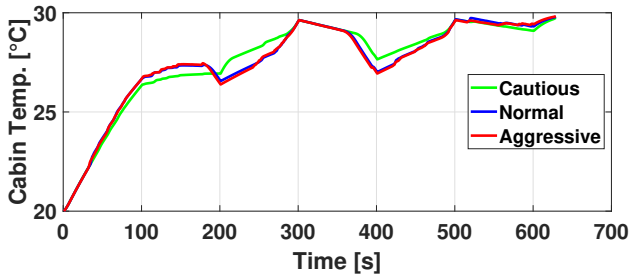

Fig. 7: Cabin temperature of different drivers with the base motor design

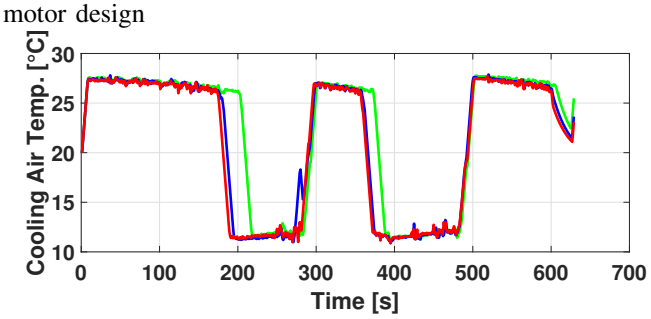

Fig. 8: Coolant temperature of different drivers with the base motor design

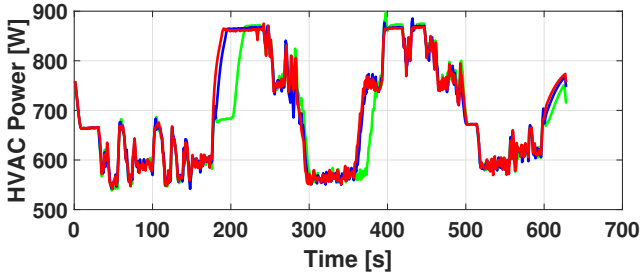

Fig. 9: HVAC power of different drivers with the base motor design

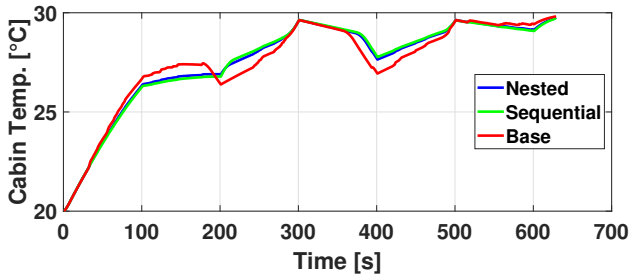

Fig. 10: Cabin temperature of the aggressive driver with three different motor designs

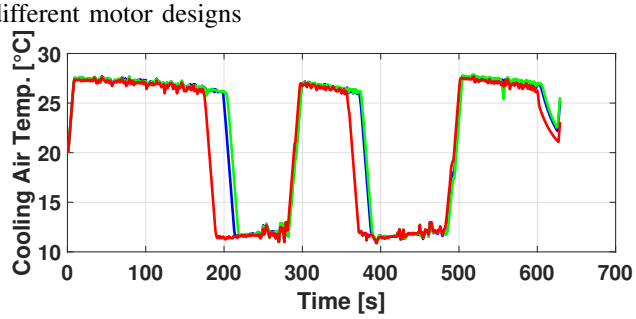

Fig. 11: Coolant temperature of the aggressive driver with three different motor designs

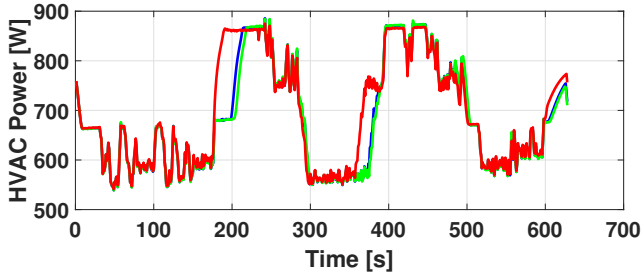

Fig. 12: HVAC power of the aggressive driver with three different motor designs

less efficient motor operations. Therefore, the vehicle should be designed considering the maximum motor torque and motor efficiency for drivability and energy saving.

In addition to the reference (base) motor which has a mass 50 kg, we obtain 6 motors through sequential and nested control co-design approaches for cautious, normal, and aggressive drivers as described in Table II. The sequential approach minimizes motor loss (8) while the nested approach minimizes total battery energy consumption while satisfying control constraints. The motors from the sequential approach, despite achieving less motor loss, are heavier than those from the nested approach. Furthermore, heavier motors are required for aggressive drivers because they operate motors in high-torque regions. The nested approach results in less total battery energy consumption by reducing motor mass in each driver characteristic.

Figs. 7-9 show the control design results of different drivers with the base motor. The aggressive driver consumes the most energy because the motor operations occur in less efficient areas compared to the other drivers, which makes cabin temperature increase and HVAC power consume more. During the period $t \in [170, 220]$s, HVAC control strategy for aggressive driver cranks up earlier than both normal and cautious drivers, way ahead of heat load spike by disturbance and motor loss. This is because the aggressive driver tends to have higher propulsive power demand, which requires the control strategy reshape the HVAC power to suppress the peak power demand on the battery.

The control design results of aggressive driver with the base motor, the motor optimized by sequential approach (sequential motor), and the motor optimized by nested approach (nested motor) are shown in Figs. 10-12. Compared to the base motor, control strategies of the sequential and nested motors reduce HVAC energy consumption by minimizing the cooling load resulted from motor loss with the more efficient motors. During the period $t \in [190, 280]$s and $t \in [370, 480]$s, the HVAC control strategy for base motor uses more HVAC power to cool down the cabin. Although the HVAC control strategy for the sequential motor reduces HVAC power compared to the nested motor by using the motor optimized for less motor loss, it consumes more battery energy in driving the vehicle due to the increased vehicle

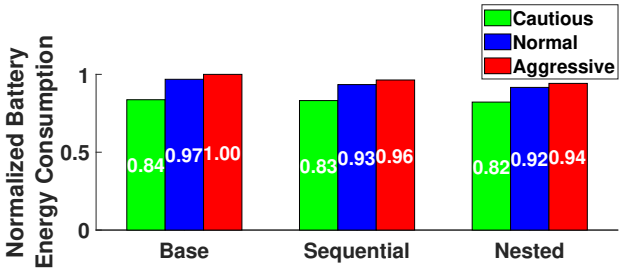

Fig. 13: Normalized battery energy consumption of different drivers with different motor designs

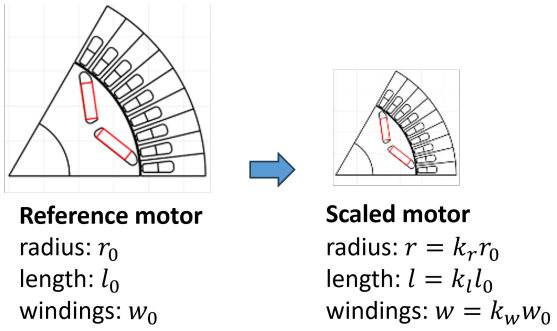

Fig. 14: Schematics of reference/scaled motors.

mass by its motor weight.

Fig. 13 describes the energy consumption of all 9 cases arising from 3 different motors and 3 different drivers. It shows that the control co-design performance improves in a more aggressive driver, which can be attributed to a more aggressive driver having more degree of freedom in motor operation to be optimized by motor design parameters and the coupling between design parameter and control strategy. The nested approach outperforms the sequential approach in achieving system-level optimality.

V. Conclusions

This research investigated the control co-design problem to tailor an electric vehicle for a driving cycle which encodes road traffic and driver characteristics. By employing real-world and driver-specific driving cycles, the resultant design and controller can be validated under realistic situations and tuned to suit customer's needs. A real-world driving cycle was synthesized in a simulation environment, which can efficiently generate road traffic information in areas of interest. Physics-based motor modeling was conducted to analytically capture the impact of motor size on system efficiency; and physics-based and data-driven modeling was performed to capture the coupling between vehicle state and HVAC power consumption. Finally, the sequential and nested co-design approaches were implemented for different driver characteristics and results were compared. Future work include battery design as well as investigate motion planning of electric vehicles for control co-design.

Appendix
Scaled Motor Modeling

Consider scaling the motor radius and length as shown in Fig. 14. Here, r_0 and l_0 are outer radius and axial length of the reference motor, respectively; k_r and k_l are the scaling factors in radius and length, respectively; r and l are the radius and length of the scaled motor, respectively. Next we investigate how each of these scaling factors works by examining the solution to the following Poisson's equation:

$$\Delta \boldsymbol{A} = -\mu_0 \boldsymbol{J} - \mu_0 \nabla \times \boldsymbol{M}, \tag{13}$$

where Δ is the Laplace operator, J is the current density, μ_0 is the air permeability, $\boldsymbol{A}$ denotes the magnetic vector potential, and $\nabla\times$ is the curl operator. Let $\boldsymbol{x}_0$ denote the coordinate of the reference motor. Given current density $\boldsymbol{J_0}(\boldsymbol{x}_0)$ and magnetization distribution $\boldsymbol{M_0}(\boldsymbol{x}_0)$, the Poisson's equation for the reference motor is written as follows

$$\Delta_{\boldsymbol{x}_0} \boldsymbol{A_0}(\boldsymbol{x}_0) = -\mu_0 \boldsymbol{J_0}(\boldsymbol{x}_0) - \mu_0 \nabla_{\boldsymbol{x}_0} \times \boldsymbol{M_0}(\boldsymbol{x}_0), \tag{14}$$

where $\nabla_{\boldsymbol{x}_0}$ means differential by the reference coordinate.

1) Radius scaling factor k_r: We would like to know how the solution $\boldsymbol{A}$ to (13) changes along with k_r. Let $\boldsymbol{x}$ be the coordinate of the scaled motor: $\boldsymbol{x} = k_r \boldsymbol{x}_0$. Poisson's equation for the scaled motor admits the same form of (14) with $\boldsymbol{x}_0$ being replaced by $\boldsymbol{x}$:

$$\Delta_{\boldsymbol{x}} \boldsymbol{A}(\boldsymbol{x}) = -\mu_0 \boldsymbol{J}(\boldsymbol{x}) - \mu_0 \nabla_{\boldsymbol{x}} \times \boldsymbol{M}(\boldsymbol{x}), \tag{15}$$

where $\nabla_{\boldsymbol{x}}$ is the differential by the scaled coordinate. We assume the vector potential A and current density J are also linearly scaled by scaling factors k_A and k_J, i.e.,

$$\boldsymbol{A}(\boldsymbol{x}) = k_A \boldsymbol{A_0}(\boldsymbol{x}_0) \tag{16a}$$
$$\boldsymbol{J}(\boldsymbol{x}) = k_J \boldsymbol{J_0}(\boldsymbol{x}_0) \tag{16b}$$
$$\boldsymbol{M}(\boldsymbol{x}) = \boldsymbol{M_0}(\boldsymbol{x}_0). \tag{16c}$$

The magnetization $\boldsymbol{M}$ is an invariant independent of scaling, because $\boldsymbol{M}$ is actually equivalent to remanent flux density B_r of the magnet, and B_r values of most practical magnets are around 1.3-1.4 Tesla, regardless of the magnet size. So, practically, $\boldsymbol{M}$ cannot be tuned.

For differential of $\boldsymbol{M}$, the relationship between the reference space and the scaled space is as follows.

$$\nabla_{\boldsymbol{x}} \times \boldsymbol{M}(\boldsymbol{x}) = \frac{\partial \boldsymbol{x}_0}{\partial \boldsymbol{x}} \nabla_{\boldsymbol{x}_0} \times \boldsymbol{M_0}(\boldsymbol{x}_0) = \frac{1}{k_r} \nabla_{\boldsymbol{x}_0} \times \boldsymbol{M_0}(\boldsymbol{x}_0) \tag{17}$$

Similarly, the differential of $\boldsymbol{A}$ is given by

$$\Delta_{\boldsymbol{x}} \boldsymbol{A}(\boldsymbol{x}) = \frac{k_A}{{k_r}^2} \Delta_{\boldsymbol{x}_0} \boldsymbol{A_0}(\boldsymbol{x}_0) \tag{18}$$

Substituting (16b), (17), and (18) into (15), we have

$$\frac{k_A}{{k_r}^2} \Delta_{\boldsymbol{x}_0} \boldsymbol{A_0}(\boldsymbol{x}_0) = -\mu_0 k_J \boldsymbol{J_0}(\boldsymbol{x}_0) - \mu_0 \frac{1}{k_r} \nabla_{\boldsymbol{x}_0} \times \boldsymbol{M_0}(\boldsymbol{x}_0),$$

which is mathematically equivalent to (14), when the following conditions are fulfilled:

$$k_A = k_r, \; k_J = k_r^{-1}. \tag{19}$$

From (19) and (16a), the magnetic field is computed by curl of $\boldsymbol{A}$, as follows:

$$\boldsymbol{B}(\boldsymbol{x}) = \nabla_{\boldsymbol{x}} \times \boldsymbol{A}(\boldsymbol{x}) = \frac{\partial \boldsymbol{x}_0}{\partial \boldsymbol{x}} \nabla_{\boldsymbol{x}_0} \times (k_A \boldsymbol{A_0}(\boldsymbol{x}_0))$$
$$= \frac{1}{k_r} \nabla_{\boldsymbol{x}_0} \times (k_A \boldsymbol{A_0}(\boldsymbol{x}_0)) \nabla_{\boldsymbol{x}_0} \times \boldsymbol{A_0}(\boldsymbol{x}_0) = \boldsymbol{B_0}(\boldsymbol{x}_0), \quad (20)$$

where $\boldsymbol{B_0}$ and $\boldsymbol{B}$ are the flux densities on the reference and scaled motor, respectively. By (20), it is shown that the reference motor and the scaled motor have the same flux density at the corresponding position, which means the magnetic saturation levels of both motors are the same.

From (19), since there is no differential of $\boldsymbol{J}$ in Poisson's equation, $\boldsymbol{J}$ is simply scaled by a factor of $\frac{1}{k_r}$. Hence, if scaling the motor size and hoping to keep the same flux density distribution, we should supply a current density by a factor of $\frac{1}{k_r}$. Since the current I is a product of the current density J and the coil area S where the coil area is scaled by ${k_r}^2$, the scaling for the current I is: $I = k_r I_0$. That means, if with k_r, to keep the same flux density distribution, we should scale the current by a factor of k_r.

Flux linkage F is the product of $\boldsymbol{B}$ and the area that the flux crosses. Since the area is a product of radius and length, the flux linkage is linearly proportional to k_r. Iron loss is linearly proportional to the iron volume, so iron loss is linearly proportional to ${k_r}^2$.

2) Length scaling factor k_l: When we ignore the axial edge effect of the motor, the field is homogeneous to the axial direction. So, $\boldsymbol{A}, \boldsymbol{M}, \boldsymbol{J}$, and $\boldsymbol{B}$ are independent of motor length. Hence, the flux linkage and iron loss are linearly proportional to k_l.

In summary, assume the reference motor has the flux linkages $F_{d0}(i_d, i_q)$ and $F_{q0}(i_d, i_q)$ in d-axis and q-axis, respectively. The aforementioned derivation allows us to establish the flux linkage of the scaled motor as follows:

$$F_d(i_d, i_q) = k_r k_l F_{d0}(\frac{i_d}{k_r}, \frac{i_q}{k_r}), \; F_q(i_d, i_q) = k_r k_l F_{q0}(\frac{i_d}{k_r}, \frac{i_q}{k_r}).$$

The inductance in d-axis and q-axis can be readily derived

$$L_d = \frac{\partial F_d(i_d, i_q)}{\partial i_d} = k_l L_{d0}, \; L_q = \frac{\partial F_q(i_d, i_q)}{\partial i_q} = k_l L_{q0}.$$

REFERENCES

[1] S. M. Lukic and A. Emadi, "Effects of drivetrain hybridization on fuel economy and dynamic performance of parallel hybrid electric vehicles," *IEEE Transactions on Vehicular Technology*, vol. 53, no. 2, pp. 385–389, 3 2004.

[2] T. Hofman, M. Steinbuch, R. van Druten, and A. F. A. Serrarens, "Design of CVT-Based Hybrid Passenger Cars," *IEEE Transactions on Vehicular Technology*, vol. 58, no. 2, pp. 572–587, 2009.

[3] H. K. Fathy, J. A. Reyer, P. Y. Papalambros, and A. G. Ulsov, "On the coupling between the plant and controller optimization problems," in *IEEE American Control Conference (ACC)*, vol. 3, 2001, pp. 1864–1869.

[4] D. J. Docimo, Z. Kang, K. A. James, and A. G. Alleyne, "A Novel Framework for Simultaneous Topology and Sizing Optimization of Complex, Multi-Domain Systems-of-Systems," *Journal of Mechanical Design*, vol. 142, no. 9, 2020.

[5] C. A. Fahdzyana, M. Salazar, and T. Hofman, "Integrated Plant and Control Design of a Continuously Variable Transmission," *IEEE Transactions on Vehicular Technology*, vol. 70, no. 5, pp. 4212–4224, 5 2021.

[6] D. R. Herber and J. T. Allison, "Nested and Simultaneous Solution Strategies for General Combined Plant and Control Design Problems," *Journal of Mechanical Design*, vol. 141, no. 1, p. 11402, 2018.

[7] S. Park and C. Ahn, "Power Management Controller for a Hybrid Electric Vehicle With Predicted Future Acceleration," *IEEE Transactions on Vehicular Technology*, vol. 68, no. 11, pp. 10 477–10 488, 2019.

[8] S. Park and C. Ahn, "Computationally Efficient Stochastic Model Predictive Controller for Battery Thermal Management of Electric Vehicle," *IEEE Transactions on Vehicular Technology*, vol. 69, no. 8, pp. 8407–8419, 2020.

[9] S. Park and C. Ahn, "Model Predictive Control With Stochastically Approximated Cost-to-Go for Battery Cooling System of Electric Vehicles," *IEEE Transactions on Vehicular Technology*, vol. 70, no. 5, pp. 4312–4323, 2021.

[10] M. Bando, K. Hasebe, A. Nakayama, A. Shibata, and Y. Sugiyama, "Dynamical model of traffic congestion and numerical simulation," *Phys. Rev. E*, vol. 51, no. 2, pp. 1035–1042, 1995.

[11] T.-K. Lee, Z. Bareket, T. Gordon, and Z. S. Filipi, "Stochastic Modeling for Studies of Real-World PHEV Usage: Driving Schedule and Daily Temporal Distributions," *IEEE Transactions on Vehicular Technology*, vol. 61, no. 4, pp. 1493–1502, 2012.

[12] M. Zhang, S. Shi, W. Cheng, and Y. Shen, "Self-Adaptive Hyper-Heuristic Markov Chain Evolution for Generating Vehicle Multi-Parameter Driving Cycles," *IEEE Transactions on Vehicular Technology*, vol. 69, no. 6, pp. 6041–6052, 2020.

[13] H. Tan, G. Feng, J. Feng, W. Wang, Y.-J. Zhang, and F. Li, "A tensor-based method for missing traffic data completion," *Transportation Research Part C: Emerging Technologies*, vol. 28, pp. 15–27, 2013.

[14] C. Miyajima, Y. Nishiwaki, K. Ozawa, T. Wakita, K. Itou, K. Takeda, and F. Itakura, "Driver Modeling Based on Driving Behavior and Its Evaluation in Driver Identification," *Proceedings of the IEEE*, vol. 95, no. 2, pp. 427–437, 2007.

[15] N. Murgovski, L. Johannesson, J. Sjöberg, and B. Egardt, "Component sizing of a plug-in hybrid electric powertrain via convex optimization," *Mechatronics*, vol. 22, no. 1, pp. 106–120, 2012.

[16] M. Pourabdollah, N. Murgovski, A. Grauers, and B. Egardt, "Optimal Sizing of a Parallel PHEV Powertrain," *IEEE Transactions on Vehicular Technology*, vol. 62, no. 6, pp. 2469–2480, 2013.

[17] M. Menner and S. Di Cairano, "Kernel Regression for Energy-Optimal Control of Fully Electric Vehicles," in *IEEE Vehicle Power and Propulsion Conference (VPPC)*, 2021, pp. 1–6.

[18] C. T. Nguyen, P. D. Walker, S. Zhou, and N. Zhang, "Optimal sizing and energy management of an electric vehicle powertrain equipped with two motors and multi-gear ratios," *Mechanism and Machine Theory*, vol. 167, p. 104513, 2022.

[19] P. A. Lopez, M. Behrisch, L. Bieker-Walz, J. Erdmann, Y.-P. Flötteröd, R. Hilbrich, L. Lücken, J. Rummel, P. Wagner, and E. Wiessner, "Microscopic Traffic Simulation using SUMO," in *IEEE International Conference on Intelligent Transportation Systems (ITSC)*, 2018, pp. 2575–2582.

[20] OpenStreetMap Contributors, "OpenStreetMap," https://www.openstreetmap.org.

[21] S. A. B. Yu Jiang Yebin Wang and Z.-P. Jiang, "An iterative approach to the optimal co-design of linear control systems," *International Journal of Control*, vol. 89, no. 4, pp. 680–690, 2016.

[22] Y. Jiang, Y. Wang, S. A. Bortoff, and Z.-P. Jiang, "Optimal Codesign of Nonlinear Control Systems Based on a Modified Policy Iteration Method," *IEEE Transactions on Neural Networks and Learning Systems*, vol. 26, no. 2, pp. 409–414, 2015.

[23] A. Wegener, M. Piórkowski, M. Raya, H. Hellbrück, S. Fischer, and J.-P. Hubaux, "TraCI: an interface for coupling road traffic and network simulators," in *Proceedings of the 11th Communications and Networking Simulation Symposium*, 2008, p. 155–163.

[24] J. A. E. Andersson, J. Gillis, G. Horn, J. B. Rawlings, and M. Diehl, "CasADi: a software framework for nonlinear optimization and optimal control," *Mathematical Programming Computation*, vol. 11, no. 1, pp. 1–36, 2019.